Inelastic Light Scattering by Multiple Vibrational Modes in Individual Gold Nanodimers

Adrien Girard, Jean Lerme, Hélène Gehan, Alain Mermet, Christophe Bonnet, Emmanuel Cottancin, Aurelien Crut, Jeremie Margueritat

Inelastic Light Scattering by Multiple Vibrational Modes in Individual Gold Nanodimers

Adrien Girard, Jean Lermé, Hélène Gehan, Alain Mermet, Christophe Bonnet, Emmanuel Cottancin, Aurélien Crut, and Jérémie Margueritat*.

Institut Lumière Matière, Université de Lyon, Université Claude Bernard Lyon 1, UMR CNRS 5306, F-69622 Villeurbanne, France

KEYWORDS Nanoparticles; Raman spectroscopy; Single-particle experiments; Nanomechanics; Acoustic coupling; Optomechanics.

ABSTRACT: To be Raman-active (or, more generally, detectable using optical spectroscopy techniques), a vibrational mode of a nanosystem has to modulate its optical response. For small, isolated nanospheres, this is the case for only two categories of vibrational modes, namely quadrupolar and radial ones. However, assembling nanospheres as dimers makes additional modes Raman-active, as previously demonstrated by the detection in the ultralow frequency range of a hybridized quasi-translation mode in previous measurements on single and ensembles of gold nanosphere dimers. In the present work, we use our recently developed single-particle Raman spectroscopy setup to compare inelastic light scattering by single isolated and dimerized gold nanospheres in an extended frequency range (0-40 GHz). The Raman spectra acquired on isolated nanoparticles present a single peak associated to their fundamental quadrupolar mode, consistently with previous ensemble measurements. In contrast, the spectra measured on dimers are richer and display a number of peaks increasing with decreasing interparticle distance, with all $l = 2 - 8$ Lamb modes detected in the quasi-contact case. These observations are rationalized using a recently developed classical model of inelastic light scattering by nanospheres. Importantly, our modeling approach takes into account the real electric field within the nanoparticles

(computed using standard or generalized Mie theories) instead of relying on the frequently used Born and quasistatic approximations. This ingredient appears decisive for reaching a qualitative understanding of the measured spectra, explaining in particular the dominance of the $l = 2$ quadrupolar mode for isolated spheres and the increasing contribution of higher-order modes for increasing electromagnetic interactions in nanosphere dimers.

The discrete acoustic vibrational modes of nano-objects have been attracting great interest for the last two decades. A key motivation underlying the study of their frequencies and damping rates is the information that they carry about the vibrating nano-objects themselves (since they depend on nano-object size[1–7], shape[8–11] and crystallinity [12–16]) and their close environment (as they are sensitive to the elastic[17,18] or viscoelastic[19] properties of the environment, the nano-object encapsulation by a solid shell[20,21] or organic ligands [22,23] and the presence of other nano-objects at vicinity [24–26]).

The vibrational properties of nano-objects are usually investigated using optical techniques working either in the time (time-resolved pump-probe spectroscopy) or frequency (Raman/Brillouin spectroscopies) domains. These two approaches strongly differ by the way vibrations are generated, since vibrational mode excitation is achieved coherently by a *pump* light pulse in the former case, and thermally in the latter one. However, these modes are detected in both cases through the modulation of the optical response of nano-objects that they induce [27–31]. Indeed, inelastic light scattering by the vibrational modes of molecules and small nanoparticles is classically interpreted in the context of Raman spectroscopy as a modulation of scattering efficiency resulting from the periodic polarizability changes that they induce[32], whereas in pump-probe spectroscopy vibrations are detected as oscillations of the transmission or reflection of a *probe* pulse measured as a function of pump-probe delay[1,2]. The strength of these modulations strongly depends on the considered nanosystem and vibrational mode. For instance, in the case of nanospheres much smaller than light wavelength, only

Lamb modes with $l = 2$ and (with a smaller intensity) $l = 0$ angular momentum numbers are detectable using Raman spectroscopy, selection rules predicting the other modes to be Raman-inactive[33].

In this context, nanoparticle dimers constitute particularly interesting systems, as they enable the detection of additional modes as compared to isolated nanoparticles. For instance, the quasi-translation vibrational modes ($l = 1$ Lamb modes) of nanospheres in a homogeneous matrix, which are not observable using Raman or time-resolved spectroscopies, become optically detectable on nanodimers[24,34] and single nanospheres above a plane substrate[35,36]. This observation qualitatively results from the modification upon nanoparticle translations of the interparticle (or particle/substrate) gap properties, which strongly affect the optical response of these systems[37–39].

In a recent work, we investigated in detail the hybridization of these $l = 1$ acoustic modes in dimers by measuring the ultra-low frequency (<15 GHz) inelastic scattering of single nanosystems (isolated nanoparticles and nanodimers)[25] and analyzing the effect of interparticle interactions on their associated frequencies, damping rates and displacement fields using numerical acoustic simulations. Here, we extend these measurements to higher frequencies (up to 45 GHz). We show in particular that single dimers made of nanoparticles in quasi-contact yield rich Raman spectra displaying several peaks in this spectral region, corresponding to acoustic modes with $l = 2$ to $l = 8$ angular momentum numbers. These experimental spectra are compared with those computed in the framework of a recently developed model of Raman scattering by nanoparticles considering the inhomogeneities of the electromagnetic field inside the nanoparticles[40], allowing a better understanding of the presence and relative amplitudes of the detected peaks.

The used nanoparticle synthesis and sample preparation methods have already been described in detail in previous reports[24,25]. The samples consist in transmission electron microscopy (TEM) substrates with a 40 nm silica membrane, on which a 5 µL drop of a diluted solution of about 100 nm diameter gold nanoparticles coated with polyvinylpyrrolidone (PVP) is deposited and left to dry for several hours. Such preparation process allows to statistically obtain nanoparticle

dimers (or more complex oligomers) separated from each other by a distance larger than 2 μm allowing their selective study using diffraction-limited optical techniques. The morphological, optical and acoustic properties of such nanodimers, as well as those of isolated single nanoparticles, were characterized using a multistep protocol. First, nanosystems of interest were located by low-magnification TEM. Second, spatial modulation spectroscopy (SMS) was used to quantitatively measure their polarization-dependent absolute extinction spectra [41]. Third, their low frequency Raman spectroscopy (LFRS) was performed at the single-nanosystem level using a 647 nm laser line. Finally, high resolution TEM observations were performed to obtain their detailed morphology. Figure 1 shows the three nanosystems considered in this work (one isolated nanoparticle and two dimers, differing by their associated inter-particle distances) as well as their respective extinction and LFRS spectra.

All the nanoparticles appearing in the TEM images shown in Figure 1 present an approximately spherical shape with a diameter of about 96 nm (see below). For the dimers, the inter-particle distance *d* varies from 6 nm (Dimer A) to distance lower than 1 nm (difficult to precisely estimate on the TEM image, Dimer B) (Figure 1b-c). The extinction spectrum of the isolated nanoparticle shows a resonance at 590 nm (Figure 1a), the spectral position predicted by Mie theory for the localized surface plasmon resonance (LSPR) of a 96 nm diameter gold nanoparticle immersed in a 1.5 refractive index (i.e. that of the PVP) homogeneous medium (see supplementary materials). The measured extinction spectra of the dimers (Figure 1b-c) present the usual characteristics of these systems (intensively investigated in the past years[16,37,42–45], and in particular a spectral separation of their longitudinal and transverse LSPRs, which can be selectively excited by aligning the incident light polarization along the dimer axis and orthogonally to it, respectively, increasing with decreasing interparticle distance). For dimer A (Figure 1b), the transverse and longitudinal resonances are observed at 530 and 630 nm, while for dimer B (Figure 1c) these peaks are observed at 570 and 750 nm, respectively. For this latter dimer, another

spectral feature is also observed at about 600 nm for light polarized along the long axis of the dimer. It corresponds to the hybridized quadrupolar mode of the dimer.

The inelastic light scattering spectra of the three investigated single nanosystems were measured for 647 nm illumination using a tandem Fabry-Perot (Figure 1d-f). The isolated nanoparticle spectrum (Figure 1d) presents a single peak at 11.0 GHz frequency, which can be unambiguously ascribed to the fundamental quadrupolar vibrational mode (corresponding to a $l = 2$ angular momentum number) of the nanoparticle. Indeed, this mode was shown to dominate inelastic scattering by ensembles of non-interacting nanospheres[9,12,14,46] and its 11.0 GHz frequency predicted by Lamb theory[47] for a 96 nm diameter gold nanosphere in vacuum (modified by <1% in an infinite PVP environment[48,49]) well matches the experimental one.

Nanoparticle dimers yield richer spectra, with two peaks observed at 11.1 and 16.6 GHz for dimer A and no less than seven at 13.4, 17.5, 20, 24, 29, 35 and 40 GHz for dimer B. Association of the vibrational frequencies measured for nanodimers to vibrational modes is *a priori* more complex than in the isolated nanoparticle case, due to the acoustic interactions between close nanoparticles induced by the presence of a PVP layer around them. In particular, our previous work on single nanodimers have demonstrated both experimentally and theoretically that the frequencies of the quasi-translational l =1 modes can be considerably shifted by this phenomenon[25]. However, reproduction of these calculations for $l = 0$ and l =2-8 modes shows that their frequencies are much less impacted by acoustic interactions, undergoing <10% shifts even in the quasi-contact case. As a consequence, Lamb theory remains a relevant approximate tool for the assignment of the observed vibrational modes. Using the sound velocities for gold of v_L=3330 m.s^{-1} and v_T=1250 m.s^{-1}, it predicts frequencies of 11.0 GHz ($l = 2$), 16.5 GHz ($l = 3$), 21.2 GHz ($l = 4$), 25.6 GHz ($l = 5$), 29.9 GHz ($l = 6$), 34.1 GHz ($l = 7$), 38.2 GHz ($l = 8$) and 32.5 GHz ($l = 0$) for the fundamental $l = 0$ and $l = 2 - 8$ vibrational modes of 96 nm

diameter gold nanospheres. Therefore, the 11.1 and 16.6 GHz peaks observed for Dimer A can be ascribed to the fundamental $l = 2$ (quadrupolar) and $l = 3$ modes. The frequencies measured for Dimer B approximately correspond to those of the $l = 2 - 8$ Lamb modes listed above (differences with the measured frequencies having at least three possible origins: deviation of nanoparticle shape from sphericity, acoustic interactions and finite PVP shell effects[20,50]).

The present observations show that assembling nanospheres as dimers allows not only to detect their quadrupolar mode using Raman spectroscopy, but also additional modes which are otherwise not Raman-active, the number of which increases with the proximity of the nanoparticles. In particular, all $l = 2 - 8$ Lamb modes can be detected for dimers in quasi-contact. Such spectral richness was already observed in opals of large silica beads[51–53], and explained by retardation effects due to the size of the beads[54]. However, it is for the first time demonstrated for metallic nanoparticles much smaller than light wavelength, for which retardation effects do not play an important role. One can speculate reasonably that the detection of multiple vibrational modes in dimers of close nanoparticles is related to electromagnetic coupling between nanoparticles, as these two effects require short interparticle distances. Nevertheless, understanding the precise mechanisms involved requires a detailed modeling of inelastic light scattering by nanoparticles. In the following, we first use the measured extinction spectra to better characterize parameters that cannot be reliably deduced from the TEM image (i.e., the local environment of the nanoparticles and the interparticle distance when it is small, as in the Dimer B case). They are then injected in a recently described classical model of inelastic light scattering by nanoparticles, describing the impact of nanoparticle vibrations on their optical response[40]. Perfectly spherical nanoparticles in a homogeneous matrix of refractive index N_m were considered in all theoretical analyses as this situation (simpler than the actual experimental one) enables analytical modeling approaches based on standard and generalized Mie theories.

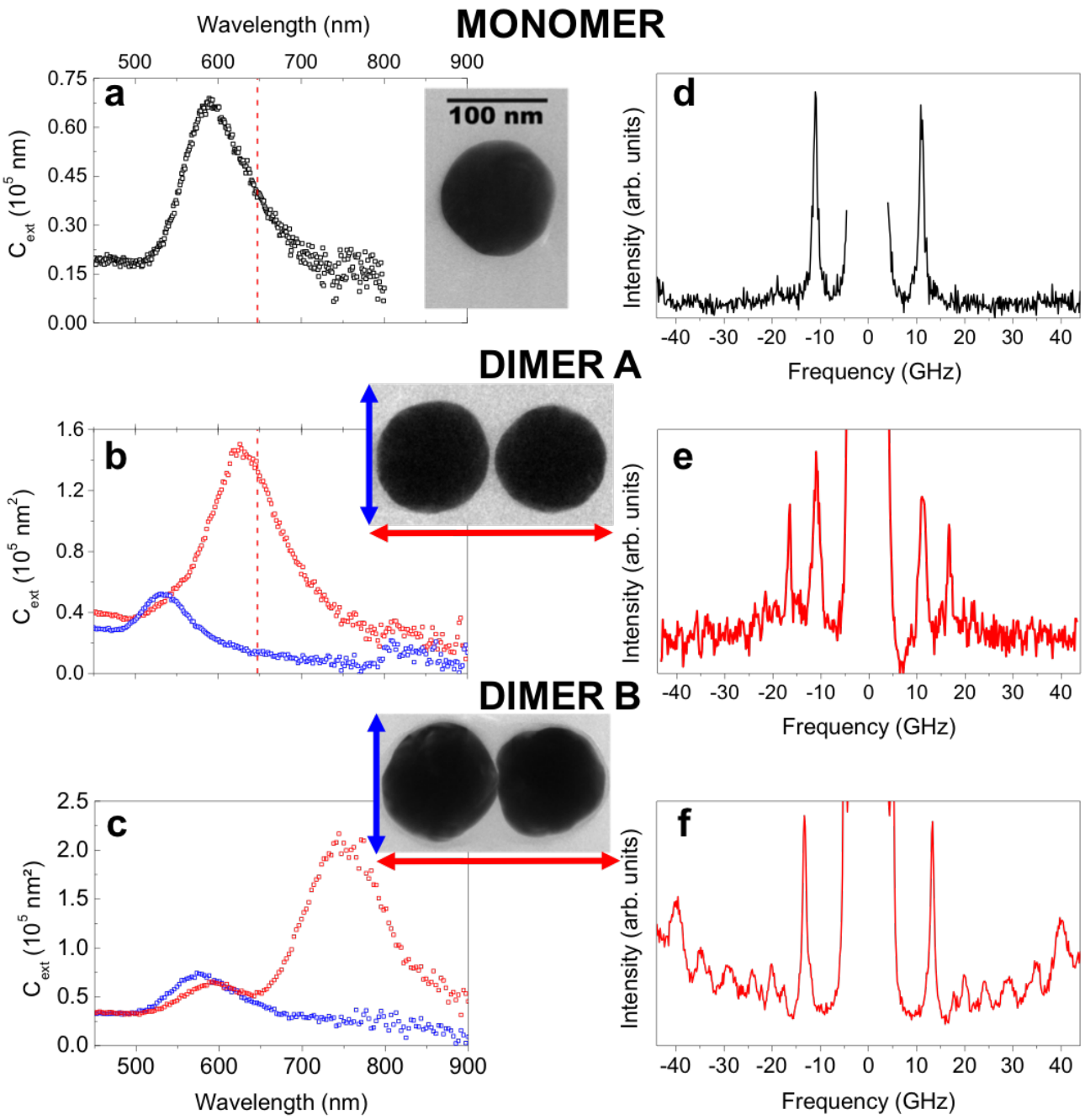

Figure 1: High resolution TEM images and extinction spectra of an isolated NP (**a.**) and two dimers with different inter-particle distances (**b.** and **c.**). No extinction dependence on the polarization of the incident light is observed for the monomer. In the dimer case, blue and red spectra were obtained by polarizing the white light along the direction perpendicular or parallel to the long axis of the dimer, respectively. **d,e,f** Low-frequency Raman scattering spectra of each considered nanosystem, measured with polarization aligned along the long axis of the dimer in **e** and **f**.

The position of the dipolar LSPR resonance of an isolated spherical nanoparticle depends on both its diameter and the effective refractive index N_m of its surrounding medium. The diameters of the investigated nanoparticles (about 96 nm) being known from their TEM images (Figure 1), it is thus possible to deduce N_m for the isolated nanoparticle (Figure 1a) from its measured extinction spectrum, by comparing it with those calculated for different N_m values using the Mie theory[55,56] (exact for any sphere size and including size-dependent retardation effects). The complex gold dielectric function measured by Johnson and Christy [57] was used for these calculations (see supplementary material). An optimal agreement is found for $N_m = 1.5$, i.e. close to the PVP refractive index in the visible spectral range[24]. Since the optical response of nanospheres is affected by their local environment on a length scale of the order of their radius, this suggests that the nanoparticle is surrounded by a PVP layer with ≥50 nm thickness.

TEM images of the considered nanodimers suggest a much thinner PVP layer around the nanoparticles (see figure 1), expected to lead to a smaller N_m value. Their measured extinction spectra were analyzed using an analytical generalized Mie theory approach, previously developed for studying gold nanodimers near the conductive contact limit[58]. The distance between the nanoparticles, d, is a crucial parameter in these analyses. It can be reliably deduced from the TEM image for dimer A ($d = 6$ nm), in which case N_m remains the only unknown parameter in the analysis, as in the isolated nanoparticle case. An optimal fit of the measured extinction spectrum of Dimer A was obtained for N_m =1.17 (a value much smaller than the PVP refractive index, as expected from the TEM image). For dimer B, d can only be estimated roughly to 1 nm or less (i.e., in a range where the dimer optical response dramatically depends on d). d has thus to be kept as a free parameter in the analysis. Assuming that the environment (i.e., the thickness of the PVP layer and the associated effective refractive index N_m) of the dimers A and B are the same, we deduce an interparticle distance d = 0.9 nm for the dimer B. However, it should be mentioned that the extinction spectrum can be reproduced by other choices of N_m and d

values, and a full discussion considering the effect of the inter-particle distance and the effective refractive index is presented in the supplementary materials.

Theoretical modeling of Raman spectra was then performed, with the goal of clarifying the origin of the multi-peak experimental dimer spectra rather than of quantitatively reproducing them (which would be challenging due to the complexity of the experimentally investigated situations and uncertainties on nanoparticle morphologies and environment). The situation enabling reproduction of the measured extinction spectra was considered in this analysis, i.e. isolated and dimerized (with in this case d=6 and 0.9 nm) 96 nm diameter gold nanospheres embedded in a homogeneous transparent medium of refractive index of N_m = 1.5 and N_m =1.17 for the monomer and the dimers, respectively.

The analysis of the Raman spectra was carried out by applying the classical formalism that we recently developed[40], built up from the standard equations of the classical radiating dipole theory and closely related to the standard classical approach for describing elastic and inelastic scattering by molecules, liquids and solids. From a microscopic point of view, the inelastic light scattering by metal particles, in the UV-VIS-NIR spectral range, results to a great extent from the time-varying changes of their core and conduction electron densities. Such density changes follow adiabatically the slow (as compared to optical frequencies) motions of the atoms about their equilibrium positions. It is therefore assumed that the local time-varying electronic susceptibility fluctuations $\delta\chi(\mathbf{r},t)$ in the homogeneous medium of density ρ_0, responsible for inelastic light scattering by acoustic vibrations, are mainly related to the tiny atomic density fluctuations $\delta\rho(\mathbf{r},t)$ according to $\delta\chi(\mathbf{r},t) = \partial\chi/\partial\rho|_{\rho_0}\delta\rho(\mathbf{r},t)$. As emphasized in our previous work,[40] such an assumption can be supported by both the Drude conduction-electron dielectric function and the Clausius-Mossoti (Lorentz-Lorenz) formulas, where the electron and dipole volume densities appear, respectively. We will limit ourselves here to mentioning the equations deduced from this hypothesis that are useful for the present analysis. More detailed information on the model can however be found in

our previous work[40], in particular the derivation of the relationship between the density fluctuations $\delta\rho_a(\mathbf{r},t)$ induced by the acoustic Lamb mode $a \equiv (l,n,m)$ and the normalized displacement field $\mathbf{u_a}(\mathbf{r})$ of this mode.

Let us consider first a single gold sphere (diameter *D*) embedded in a homogeneous transparent matrix of dielectric index N_m subject to an incoming monochromatic linearly-polarized plane wave $\mathbf{E_0}(\mathbf{r},t) = \mathbf{E_0}e^{i(\boldsymbol{k_0}\cdot\boldsymbol{r}-\boldsymbol{\omega_0 t})}$ (for convenience the origin O is taken at the sphere center). The contribution of each Lamb mode $a \equiv (l,n,m)$ (with l, n and m the angular momentum, radial and azimuthal numbers, respectively) to the Stokes part of the **m**-polarized ($\mathbf{m}\cdot\mathbf{u} = 0$) Raman spectrum recorded at the position P (in the direction **u**) writes as

$$I(a) \propto \frac{1+n(\omega_a)}{\omega_a}\left|\mathbf{m}\cdot\left(\mathbf{u}\times\left(\mathbf{u}\times\left(\int d^3r\mathbf{E_{int}}(\mathbf{r})e^{-i\mathbf{k}\cdot\mathbf{r}}\frac{\partial\delta\rho_a(\mathbf{r})}{\partial Q_a}\right)\right)\right)\right|^2 \quad (1)$$

with

$$\frac{\partial\delta\rho_a(\mathbf{r})}{\partial Q_a} \propto [H(R-|\mathbf{r}|)\nabla\cdot\mathbf{u}_a^*(\mathbf{r}) - \delta(r-R)\mathbf{u}_a^*(\mathbf{r})\cdot\mathbf{e}_r] \quad (2)$$

where Q_a is the normal coordinate of the a-mode.

In the above equations, only the factors relevant for computing the relative Raman intensities for a fixed excitation wavelength are given. $n(\omega_a)$ is the Bose-Einstein occupancy function (T = 300 K temperature was assumed throughout this work) and ω_a the angular frequency of the mode a, $\mathbf{u} = \mathbf{OP}/|\mathbf{OP}| = \mathbf{k}/|\mathbf{k}|$ and $\mathbf{k} = (2\pi N_m/\lambda_0)\mathbf{u} = (N_m\omega_0/c)\mathbf{u}$ is the scattered wave-vector. $\mathbf{e}_r$ is the outward-pointing unit vector normal to the surface of the sphere. *H*(x) is the Heaviside step function (*H*(*x*) = 1 for *x* > 0 and *H*(*x*) = 0 for *x* < 0) and $\delta(x)$ the Dirac function.

From the analytical expression of the displacement field of the vibrational mode $a \equiv (l,n,m)$ [59], the $\partial\delta\rho_a(\mathbf{r})/\partial Q_a$ term in eqs (1) and (2) can be expressed as the sum of volume ($g_{l,n}^{(V)}(\mathrm{r})$) and surface ($g_{l,n}^{(S)}(\mathrm{r})$) terms

$$\frac{\partial\delta\rho_a(\mathbf{r})}{\partial Q_a} \propto \left[g_{l,n}^{(V)}(\mathrm{r}) + \delta(\mathrm{r}-R)g_{l,n}^{(S)}(\mathrm{r})\right]Y_l^{m^*}(\theta,\phi) \quad (3)$$

The **r**-dependence of the product $\mathbf{E_{int}}(\mathbf{r})e^{-i\mathbf{k}\cdot\mathbf{r}}$ appearing in eq (1), which weights the individual wavelets scattered by each volume element of the sphere, is a key ingredient of the model. In particular, in view of eqs. (1) and (3), and of the orthogonality properties of the scalar spherical harmonics, only the components of the product $\mathbf{E}_{\mathrm{int}}(\mathbf{r})e^{-i\mathbf{k}\cdot\mathbf{r}}$ of angular symmetry $Y_l^m(\theta,\phi)$ will contribute to the inelastic scattering from the mode a. Importantly, $\mathbf{E}_{\mathrm{int}}(\mathbf{r})$ represents the *real* driving internal electric field responsible for the high-frequency "dipole radiation" in eq (1). In our formalism this field is exactly computed thanks to Mie theory, yielding its actual magnitude, phase and spatial inhomogeneities, rather than by resorting to either Born ($\mathbf{E_0}\, e^{i\mathbf{k_0}\cdot\mathbf{r}}$ taken in place of $\mathbf{E}_{\mathrm{int}}(\mathbf{r})$) or quasistatic (neglecting spatial variations of the incoming field in the nanosphere volume, which leads to uniform $\mathbf{E}_{\mathrm{int}}(\mathbf{r})$) approximations. Note that $\mathbf{E}_{\mathrm{int}}(\mathbf{r})$ implicitly includes the position-dependent phase factor of the incoming field, so that the exchanged wave-vector $\mathbf{q} = \mathbf{k}_0 - \mathbf{k}$ does not appear explicitly in eq (1).

It should be emphasized that our modeling is indeed closely related to the Brillouin mechanism described for instance in refs[29,60] in the frame of atomistic approaches, although the fluctuations of the density of microscopic polarization units do not appear *explicitly* in these models. The major difference between our formalism and standard atomistic approaches follows from a more precise description of the driving Rayleigh field responsible for the "dipole radiation", and thus for elastic and inelastic scattering processes. Indeed, in the usual atomistic Brillouin/Raman scattering models the Born approximation, or at least the homogeneity of the driving Rayleigh field, is implicitly assumed (neglecting moreover the phase factor $e^{-i\mathbf{k}\cdot\mathbf{r}}$ in the case of sub-wavelength particle size), even in the case of dense systems as solids or liquids[27–29,60,61]. These models, taking into account only the variation of the phase factor $e^{i\mathbf{q}\cdot\mathbf{r}}$, were used successfully for the analysis of inelastic light scattering experiments performed on large dielectric nanoparticles[51], but were rarely applied to the analysis of LFRS measurements on metallic nanoparticles[5,9,10,62], the observed modes being generally identified by

considering only the selection rules.[33] The simple model we developed provides a unified picture for describing the Brillouin scattering-related mechanism for any material, suitable for handling both small and large sizes, as well as non-resonant and resonant excitation conditions in the case of plasmonic particles.

Throughout this work, we compute the unpolarized Raman spectrum collected in backscattering geometry for a λ_0 = 647 nm excitation wavelength (all the technical aspects associated to these calculations will be reported in a forthcoming theoretical paper). The Lamb modes of free spheres (computed for stress-free boundary conditions at the nanosphere surface) were considered in our simulations[59]. Omitting environment effects (and, in the dimer case, acoustic interaction ones) appears reasonable here, as acoustic numerical simulations (determined using the same procedure as in our previous work[25]) show that they lead to modest frequency shifts for the l=0 and l=2-8 vibrational modes considered here, in strong contrast with the l=1 mode case considered in our previous works[24,25]. Note that each Raman peak is the sum of $2l+1$ contributions because of the m-degeneracy of the Lamb modes (the frequency depends only on l and n). In order to facilitate the comparison between experimental and simulated inelastic scattering spectra, each computed Raman peak was convoluted with a narrow mode-independent Lorentzian-shape curve with a full width at half-maximum (FWHM) $\Delta\omega = 1.5$ GHz (actual damping rates being inaccessible using Lamb theory).

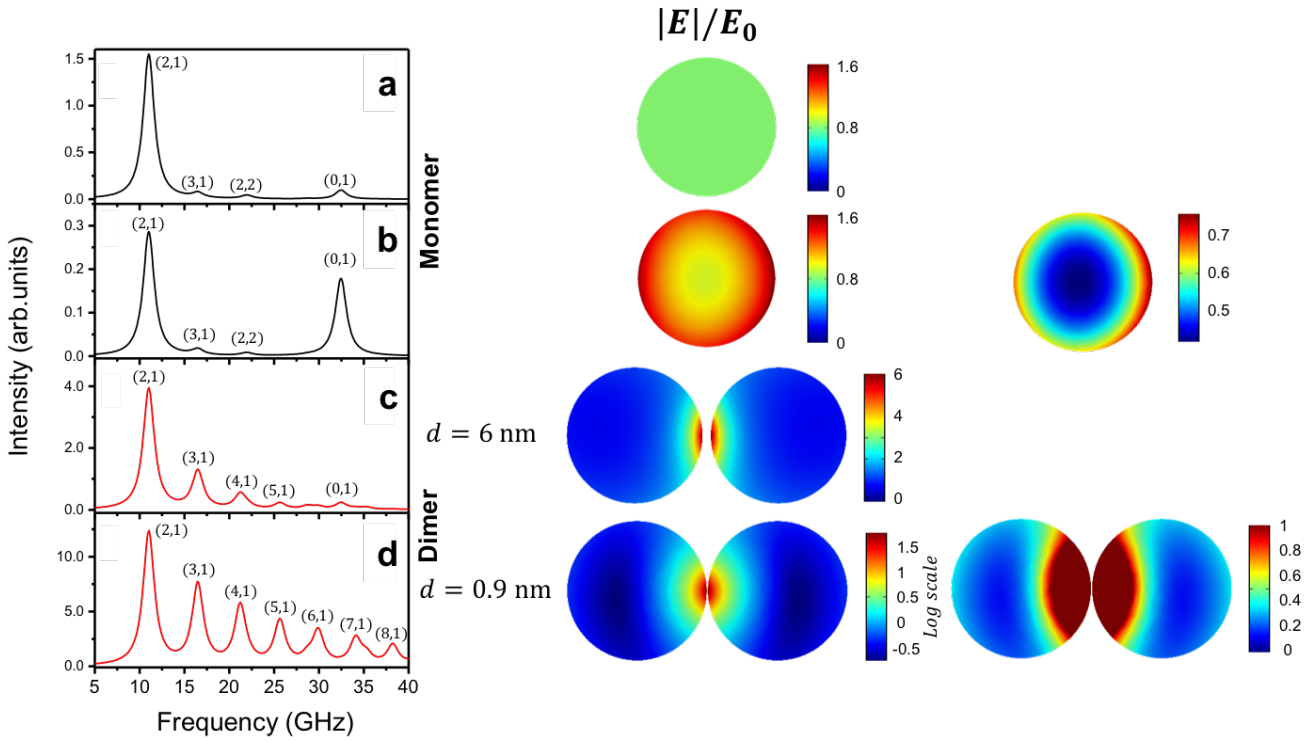

Figure 2: Calculated unpolarized Raman spectra of isolated and dimerized $D = 96$ nm diameter gold nanospheres embedded in a homogeneous matrix of refractive index $N_m = 1.5$ (monomer) and $N_m = 1.17$ (dimer). The spectra are collected in backscattering geometry, for the $\lambda_0 = 647$ nm Rayleigh excitation wavelength. Each Raman line (l, n) has been convoluted with a Lorentzian-shape curve (full width at half-maximum equal to $\Delta\omega = 1.5$ GHz). The normalized driving internal Rayleigh fields $\mathbf{E}_{\text{int}}(\mathbf{r})$ inside the gold spheres are shown on the right for each considered situation. (a-b): isolated nanosphere, with $\mathbf{E}_{\text{int}}(\mathbf{r})$ computed using Born approximation ($\mathbf{E}_{\text{int}}(\mathbf{r}) = \mathbf{E}_0 e^{i\mathbf{k}_0 \cdot \mathbf{r}}$, (a)) and Mie theory with different color scales(b). (c-d) Dimers with d=6 nm (c) and d=0.9 nm (d) interparticle distances. $\mathbf{E}_{\text{int}}(\mathbf{r})$ was computed thanks to the generalized Mie theory in both cases. Some field distributions are shown with different scales to emphasize the field inhomogeneity.

Computed Raman spectra of an isolated gold sphere of 96 nm diameter embedded in a homogeneous matrix of refractive index N_m = 1.5, are plotted in Figure 2a-b. In Figure 2a is displayed the Raman spectrum of the sphere obtained

in the context of Born approximation, i.e., replacing the real internal field $\mathbf{E}_{int}(\mathbf{r})$ by the applied one $\mathbf{E}_0 e^{i\mathbf{k_0}\cdot\mathbf{r}}$, leading to a perfectly uniform internal field amplitude inside the nanoparticle. The calculated spectrum in Figure 2a, dominated by the fundamental quadrupolar mode, is in agreement with the measured spectra in previous experiments[5,9,10,62] performed on small nanoparticles (<5 nm) in which the internal electric field can actually be considered as uniform. Considering the exact distribution of the internal field (Figure 2b), i.e. when each polarizable volume element of the *isolated* sphere is subject to the exact driving Rayleigh field, leads to an inelastic spectrum with a shape similar to the one calculated using the Born approximation, at the exception of a modification of the $I_{l=2}/I_{l=0}$ intensity ratio.

In contrast, including the exact internal field distribution in the modeling is absolutely essential for achieving a reasonable reproduction of the inelastic spectra of dimers of close nanoparticles (Figure 2). Figure 2 c-d shows the Raman spectra computed for dimers of gold nanospheres (assuming that they vibrate incoherently) separated by $d = 6$ nm and $d = 0.9$ nm. In this case, electromagnetic interactions occur between the two spheres, with a strength increasing with decreasing d, and each sphere is illuminated not only by the incoming wave ($\mathbf{E}_0$ field), but also by the inhomogeneous near-field produced by the other sphere. As a result, strong field inhomogeneities, involving numerous multipolar components, develop inside the spheres for small separating distances, as shown on the field maps in Figure 2. For instance, strong inhomogeneity of the internal field $\mathbf{E_{int}}(\mathbf{r})$ is indeed observed in each gold sphere (very localized hot-spots) for d=0.9 nm (Figure 2d) when the polarization of the incident electric field $\mathbf{E_0}(\mathbf{r}, t)$ is parallel to the dimer axis (longitudinal excitation). The plasmonic coupling between the spheres leads to two major conspicuous effects regarding their inelastic scattering, namely the emergence of high angular momentum Lamb mode contributions and an enhancement of the Raman intensity over the entire frequency range. Fundamental modes $(n = 1)$ of a broad range of angular momenta (up to $l = 8$) become observable on the simulated spectra as d is decreased. Some harmonic modes $(n = 2)$ can also be distinguished, but their contributions are very weak. The fundamental quadrupolar mode $(l = 2, n = 1)$ remains the

dominant contribution to the Raman spectrum. In contrast, the Raman activity of the fundamental radial mode $(l = 0, n = 1)$ is almost completely quenched in this system. A steady, and rather steep, decrease of the Raman intensity of the fundamental mode sequence $(l \geq 2, n = 1)$ with increasing l-value is also clearly observed. This trend is to a large extent due to the factor $(1 + n(\omega_a))/\omega_a$ appearing in eq (1), which scales as $1/\omega_a^2$ at room temperature and in the acoustic frequency range involved.

The predicted spectra are in good qualitative agreement with the experimental ones, especially regarding the number and nature of detected modes in the 5-40 GHz range, demonstrating the interest of our model for a better understanding of inelastic scattering signals. In particular, the detection of $l = 2$-3 for Dimer A and $l = 2$-8 modes for Dimer B is well explained by our model, which predicts these modes to be the dominant ones in the d=6 nm and d=0.9 nm cases. Nevertheless, the agreement with the experimental spectra is less good regarding the relative intensities of the Raman peaks. These discrepancies probably originate in part from the simplifications made in the analysis (consideration of perfectly spherical nanoparticles in a homogeneous environment). Additionally, other mechanisms as that considered in our model, such as the so-called Raman term of the atomistic models, which gathers several scattering mechanisms of various nature, contribute to the inelastic scattering[28,29,60]. Among them the dipole induce dipole (DID) mechanism, which is predicted to promote essentially the Raman quadrupolar mode contribution in dielectric nanocrystals of various structures[27]. Another mechanism disregarded in our modeling, as in existing atomistic models, is the multiple scattering of the Stokes and anti-Stokes photons/waves inside the particle. The effect of DID and multiple scattering mechanisms, that are also strongly related to the exact distribution of the internal field $\mathbf{E}_{\mathrm{int}}(\mathbf{r})$ inside the nanoparticle, are discussed in detail in the supplementary materials. In particular, the inclusion of multiple scattering mechanism through a simple phenomenological approach is shown to improve the agreement between experimental and theoretical Raman spectra.

The dimer spectra strongly contrast with that of the isolated nanoparticle, which only exhibits the two fundamental modes (l=2 and l=0) predicted from symmetry arguments in the quasistatic limit (homogeneous driving field)[33]. This result clearly demonstrates the central role played by the inhomogeneity of the driving Rayleigh field inside the scattering medium, which promotes the Raman activity of high angular momentum Lamb modes. In the present system, the source of the inhomogeneity in each (rather small) particle is the plasmonic coupling with the neighboring partner, in contrast to the case of previous theoretical studies where the emergence of high angular momenta results from the retardation effects associated to the large size of the investigated particles[29]. It has to be noted that our model can also be successfully applied to larger nanoparticles of different materials.

In conclusion, we have experimentally measured the inelastic light scattering by single nanosystems (isolated and dimerized gold nanospheres) over a broad frequency range. Efficient scattering by high angular momentum Lamb modes has been demonstrated for the first time in such small systems in the case of dimers, and is shown to increase with decreasing interparticle distance. The calculations carried out for the considered nanosystems point out that the involvement of the exact driving Rayleigh field $\mathbf{E_{int}}(\mathbf{r})$, which constitutes the originality of our model, is a key ingredient for interpreting inelastic scattering by the vibrational modes of electromagnetically coupled metal nanoparticles, in which $\mathbf{E_{int}}(\mathbf{r})$ is highly inhomogeneous. Additionally, they also show that assembling nanoparticles as dimers increases both the number of their Raman-active modes and the efficiency of their inelastic scattering, thus providing more detailed and more easily accessible information on their mechanical properties.

Our model enables a good reproduction of the trends observed in the reported experiments, and more generally a better understanding of Raman scattering (note that it is not limited to the case of small metal nanoparticles and could be applied to other nanoparticle size/composition). However, it is restricted to the Brillouin related mechanism and could be further refined by including two additional ingredients: first the Raman term of the atomistic models, which gathers the

DID contribution and the local changes of the intrinsic microscopic polarizabilities induced by the vibrations, and second the multiple scattering processes affecting the Stokes and anti-Stokes photons. Moreover, building a full opto-mechanical model of Raman scattering by nanoparticle dimers (or oligomers) simultaneously taking into account electromagnetic (as here) and acoustic (as in our previous works[24,25]) interactions between close nanoparticles would be useful to address in more detail the inelastic scattering by l=1 Lamb modes, which are highly affected by acoustic hybridization.

ASSOCIATED CONTENT

Supporting Information

Determination of the input parameters; analysis of the extinction cross-sections; analysis of the Low Frequency Raman Spectra (LFRS) of the monomer, dimer A and dimer B; dependence of the LFSR on the inter-particle distance in dimers; comments about the dipole-induced-dipole mechanism; phenomenological modeling of the multiple scattering of the Stokes and anti-Stokes photons. This material is available free of charge via the Internet at http://pubs.acs.org.

AUTHOR INFORMATION

Corresponding Author

* E-mail: jeremie.margueritat@univ-lyon1.fr

Present Addresses

Dr. Adrien Girard present address: MONARIS, UMR 8233, Université Pierre et Marie Curie, 4 Place Jussieu, Case 49, F-75252 Paris Cedex 05, France

Funding Sources

This work was supported by the ANR NanoVip project, Grant ANR.13.JS10.0002 of the French Agence National de la Recherche and the Fédération André Marie Ampère 2013 (FRAMA).

Notes

The authors declare no competing financial interest.

ACKNOWLEDGMENT

We thank the Centre Technologique des Microstructures at Villeurbanne for access to its TEM microscopy platform.

REFERENCES

1. Hodak, J. H., Martini, I. & Hartland, G. V. Spectroscopy and Dynamics of Nanometer-Sized Noble Metal Particles. *J. Phys. Chem. B* **102**, 6958–6967 (1998).
2. Del Fatti, N., Voisin, C., Chevy, F., Vallée, F. & Flytzanis, C. Coherent acoustic mode oscillation and damping in silver nanoparticles. *J. Chem. Phys.* **110**, 11484–11487 (1999).
3. Juvé, V. *et al*. Probing Elasticity at the Nanoscale: Terahertz Acoustic Vibration of Small Metal Nanoparticles. *Nano Lett.* **10**, 1853–1858 (2010).
4. Fujii, M., Nagareda, T., Hayashi, S. & Yamamoto, K. Low-frequency Raman scattering from small silver particles embedded in SiO_2 thin films. *Phys. Rev. B* **44**, 6243–6248 (1991).
5. Duval, E. *et al*. Spatial coherence effect on the low-frequency Raman scattering from metallic nanoclusters. *Phys. Rev. B* **63**, 075405 (2001).
6. Portales, H. *et al*. Resonant Raman scattering by breathing modes of metal nanoparticles. *J. Chem. Phys.* **115**, 3444 (2001).

7. Bachelier, G., Margueritat, J., Mlayah, A., Gonzalo, J. & Afonso, C. N. Size dispersion effects on the low-frequency Raman scattering of quasispherical silver nanoparticles: Experiment and theory. *Phys. Rev. B* **76**, 235419 (2007).

8. Hu, M. *et al*. Vibrational Response of Nanorods to Ultrafast Laser Induced Heating: Theoretical and Experimental Analysis. *J. Am. Chem. Soc.* **125**, 14925–14933 (2003).

9. Margueritat, J. *et al*. From silver nanolentils to nanocolumns: surface plasmon–polaritons and confined acoustic vibrations. *Appl. Phys. A* **89**, 369–372 (2007).

10. Margueritat, J. *et al*. Surface Plasmons and Vibrations of Self-Assembled Silver Nanocolumns. *Nano Lett.* **6**, 2037–2042 (2006).

11. Pelton, M. *et al*. Damping of acoustic vibrations in gold nanoparticles. *Nat. Nanotechnol.* **4**, 492–495 (2009).

12. Portalès, H. *et al*. Crystallinity Segregation upon Selective Self-Assembling of Gold Colloidal Single Nanocrystals. *Nano Lett.* **12**, 5292–5298 (2012).

13. Portales, H. *et al*. Probing atomic ordering and multiple twinning in metal nanocrystals through their vibrations. *Proc. Natl. Acad. Sci.* **105**, 14784–14789 (2008).

14. Stephanidis, B. *et al*. Vibrations of nanoparticles: From nanospheres to fcc cuboctahedra. *Phys. Rev. B* **76**, 3–6 (2007).

15. Crut, A., Maioli, P., Fatti, N. Del & Vallée, F. Anisotropy effects on the time-resolved spectroscopy of the acoustic vibrations of nanoobjects. *Phys. Chem. Chem. Phys.* **11**, 5882 (2009).

16. Yi, C. *et al*. Polycrystallinity of Lithographically Fabricated Plasmonic Nanostructures Dominates Their Acoustic Vibrational Damping. *Nano Lett.* **18**, 3494–3501 (2018).

17. Voisin, C., Christofilos, D., Del Fatti, N. & Vallée, F. Environment effect on the acoustic vibration of metal nanoparticles. *Phys. B Condens. Matter* **316–317**, 89–94 (2002).

18. Girard, A. *et al*. Contact laws between nanoparticles: the elasticity of a nanopowder. *Nanoscale* **10**, 2154–2161 (2018).

19. Pelton, M., Chakraborty, D., Malachosky, E., Guyot-Sionnest, P. & Sader, J. E. Viscoelastic Flows in Simple Liquids Generated by Vibrating Nanostructures. *Phys. Rev. Lett.* **111**, 244502 (2013).

20. Mongin, D. *et al*. Acoustic vibrations of metal-dielectric core-shell nanoparticles. *Nano Lett.* **11**, 3016–21 (2011).

21. Fernandes, B. D. *et al*. Acoustic Vibrations of Core-Shell Nanospheres: Probing the Mechanical Contact at the Metal-Dielectric Interface. *J. Phys. Chem. C* **122**, 9127–9133 (2018).

22. Girard, A. *et al*. The mass load effect on the resonant acoustic frequencies of colloidal semiconductor nanoplatelets. *Nanoscale* **8**, 13251–13256 (2016).

23. Girard, A. *et al*. Environmental effects on the natural vibrations of nanoplatelets: a high pressure study. *Nanoscale* **9**, 6551–6557 (2017).

24. Girard, A. *et al*. Mechanical Coupling in Gold Nanoparticles Supermolecules Revealed by Plasmon-Enhanced Ultralow Frequency Raman Spectroscopy. *Nano Lett.* **16**, 3843–3849 (2016).

25. Girard, A. *et al*. Acoustic Mode Hybridization in a Single Dimer of Gold Nanoparticles. *Nano Lett*. **18**, 3800–3806 (2018).

26. Yi, C. *et al*. Vibrational coupling in plasmonic molecules. *Proc. Natl. Acad. Sci*. **114**, 11621–11626 (2017).

27. Mattarelli, M., Montagna, M., Rossi, F., Chiasera, A. & Ferrari, M. Mechanism of low-frequency Raman scattering from the acoustic vibrations of dielectric nanoparticles. *Phys. Rev. B* **74**, 153412 (2006).

28. Montagna, M. & Dusi, R. Raman scattering from small spherical particles. *Phys. Rev. B* **52**, 10080–10089 (1995).

29. Montagna, M. Brillouin and Raman scattering from the acoustic vibrations of spherical particles with a size comparable to the wavelength of the light. *Phys. Rev. B* **77**, 045418 (2008).

30. Crut, A., Maioli, P., Del Fatti, N. & Vallée, F. Acoustic vibrations of metal nano-objects: Time-domain investigations. *Phys. Rep*. **549**, 1–43 (2015).

31. Ahmed, A., Pelton, M. & Guest, J. R. Understanding How Acoustic Vibrations Modulate the Optical Response of Plasmonic Metal Nanoparticles. *ACS Nano* **11**, 9360–9369 (2017).

32. Herzberg, G. *Molecular Spectra and Molecular Structure: Spectra of diatomic molecules, Volume 1, second edition*. (D. Van Nostrand Compagny, Inc., 1945).

33. Duval, E. Far-infrared and Raman vibrational transitions of a solid sphere: Selection rules. *Phys. Rev. B* **46**, 5795–5797 (1992).

34. Tchebotareva, A. L. *et al*. Acoustic and Optical Modes of Single Dumbbells of Gold Nanoparticles. *ChemPhysChem* **10**, 111–114 (2009).

35. Guillet, Y., Audoin, B., Ferrié, M. & Ravaine, S. All-optical ultrafast spectroscopy of a single nanoparticle-substrate contact. *Phys. Rev. B* **86**, 35456 (2012).

36. Deacon, W. M. *et al*. Interrogating Nanojunctions Using Ultraconfined Acoustoplasmonic Coupling. *Phys. Rev. Lett*. **119**, 1–5 (2017).

37. Nordlander, P., Oubre, C., Prodan, E., Li, K. & Stockman, M. I. Plasmon hybridization in nanoparticle dimers. *Nano Lett*. **4**, 899–903 (2004).

38. Sönnichsen, C., Reinhard, B. M., Liphardt, J. & Alivisatos, A. P. A molecular ruler based on plasmon coupling of single gold and silver nanoparticles. *Nat. Biotechnol*. **23**, 741–745 (2005).

39. Benz, F. *et al*. Nanooptics of molecular-shunted plasmonic nanojunctions. *Nano Lett*. **15**, 669–674 (2015).

40. Girard, A., Lermé, J., Gehan, H., Margueritat, J. & Mermet, A. Mechanisms of resonant low frequency Raman scattering from metallic nanoparticle Lamb modes. *J. Chem. Phys*. **146**, 194201 (2017).

41. Billaud, P. *et al*. Absolute optical extinction measurements of single nano-objects by spatial modulation spectroscopy using a white lamp. *Rev. Sci. Instrum*. **81**, 1–12 (2010).

42. Lermé, J. Plasmon Hybridization Model for a Nanoparticle above a Dielectric Interface: Dielectric

Effects, Comparison with the Dimer System, Range of Applicability, and Limits. *J. Phys. Chem. C* **119**, 21087–21104 (2015).

43. Lermusiaux, L., Maillard, V. & Bidault, S. Widefield spectral monitoring of nanometer distance changes in DNA-templated plasmon rulers. *ACS Nano* **9**, 978–990 (2015).

44. Lombardi, A. *et al*. Optical Response of Individual Au-Ag@SiO2 Heterodimers. *ACS Nano* **7**, 2522–2531 (2013).

45. Prodan, E., Radloff, C., Halas, N. J. & Nordlander, P. A hybridization model for the plasmon response of complex nanostructures. *Science (80-.).* **302**, 419–22 (2003).

46. Courty, a, Mermet, A., Albouy, P. a, Duval, E. & Pileni, M. P. Vibrational coherence of self-organized silver nanocrystals in f.c.c. supra-crystals. *Nat. Mater.* **4**, 395–398 (2005).

47. Lamb, H. On the Vibrations of an Elastic Sphere. *Proc. London Math. Soc.* **s1-13**, 189–212 (1881).

48. Dubrovskiy, V. S. & Morochnik, V. A. Natural vibrations of a spherical inhomogeneity in an elastic medium. *Phys. Solid Earth* **17**, 494–504 (1981).

49. Saviot, L., Netting, C. H. & Murray, D. B. Damping by Bulk and Shear Viscosity of Confined Acoustic Phonons for Nanostructures in Aqueous Solution. *J. Phys. Chem. B* **111**, 7457–7461 (2007).

50. Crut, A. *et al*. Vibrations of spherical core-shell nanoparticles. *Phys. Rev. B* **83**, 205430 (2011).

51. Mattarelli, M., Montagna, M., Still, T., Schneider, D. & Fytas, G. Vibration spectroscopy of weakly interacting mesoscopic colloids. *Soft Matter* **8**, 4235 (2012).

52. Kuok, M. H., Lim, H. S., Ng, S. C., Liu, N. N. & Wang, Z. K. Brillouin Study of the Quantization of Acoustic Modes in Nanospheres. *Phys. Rev. Lett.* **90**, 255502 (2003).

53. Li, Y. *et al*. Micro-Brillouin scattering from a single isolated nanosphere. *Appl. Phys. Lett.* **88**, 023112 (2006).

54. Still, T., Mattarelli, M., Kiefer, D., Fytas, G. & Montagna, M. Eigenvibrations of Submicrometer Colloidal Spheres. *J. Phys. Chem. Lett.* **1**, 2440–2444 (2010).

55. Mie, G. Beiträge zur Optik trüber Medien, speziell kolloidaler Metallösungen. *Ann. Phys.* **330**, 377–445 (1908).

56. Bohren, C. F. & Huffman, D. R. *Absorption and Scattering of Light by Small Particles*. (Wiley-VCH Verlag GmbH, 1998). doi:10.1002/9783527618156

57. Johnson, P. B. & Christy, R. W. Optical constants of the noble metals. *Phys. Rev. B* **6**, 4370–4379 (1972).

58. Marhaba, S. *et al*. Surface Plasmon Resonance of Single Gold Nanodimers near the Conductive Contact Limit. *J. Phys. Chem. C* **113**, 4349–4356 (2009).

59. Eringen, A. C. & Suhubi, E. S. *Elastodynamics Vol.II: Linear Theory*. (Elsevier, 1975). doi:10.1016/C2013-0-10628-9

60. Benassi, P. *et al*. Disorder-induced light scattering in solids: Microscopic theory and applications to some model systems. *Phys. Rev. B* **44**, 11734–11742 (1991).

61. Mazzacurati, V. *et al*. Vibrational dynamics and Raman scattering in fractals: A numerical study. *Phys. Rev. B* **45**, 2126–2137 (1992).

62. Palpant, B. *et al*. Quadrupolar vibrational mode of silver clusters from plasmon-assisted Raman scattering. *Phys. Rev. B* **60**, 17107–17111 (1999).

SYNOPSIS TOC (Word Style “SN_Synopsis_TOC”). If you are submitting your paper to a journal that requires a synopsis graphic and/or synopsis paragraph, see the Instructions for Authors on the journal’s homepage for a description of what needs to be provided and for the size requirements of the artwork.